THE AMERICAN SOCIETY OF MECHANICAL ENGINEERS
345 E. 47th St., New York, N.Y. 10017

98-GT-107

EFFECT OF HIGH FREESTREAM TURBULENCE WITH LARGE LENGTH SCALE ON BLADE HEAT/MASS TRANSFER

H. P. Wang, R. J. Goldstein and S. J. Olson

Department of Mechanical Engineering
University of Minnesota
Minneapolis, MN 55455, U.S.A.

ABSTRACT

The naphthalene sublimation technique is used to investigate the influence of high freestream turbulence with large length scale on the heat/mass transfer from a turbine blade in a highly accelerated linear cascade. The experiments are conducted at four exit Reynolds numbers, ranging from 2.4×10^5 to 7.8×10^5, with freestream turbulence of 3%, 8.5% and 18% and corresponding integral length scales of 0.9 cm, 2.6 cm and 8 cm, respectively. On the suction surface, the heat/mass transfer rate is significantly enhanced by high freestream turbulence due to an early boundary layer transition. By contrast, the transition occurs very late, and may not occur at very low Reynolds numbers with low freestream turbulence. In the turbulent boundary layer, lower heat/mass transfer rates are found for the highest freestream turbulence level with large length scale than for the moderate turbulence levels with relatively small scales. Similar phenomena also occur at the leading edge. However, the effect of turbulence is not as pronounced in the laminar boundary layer.

NOMENCLATURE

A_1	inlet area of one flow passage, see Fig. 2, $= PH\cos\beta_1$
A_2	outlet area of one flow passage, see Fig. 2, $= PH\cos\beta_2$
a_1	dimensionless strain rate, $U_\infty = a_1 U_{in} x/D$ for flow near the leading edge of a circular cylinder, =4 for potential flow
C	chord length of blade, = 18.4 cm
C_{Ps}	static pressure coefficient,
C_x	axial chord of blade, = 13.0 cm
D	diffusion coefficient of naphthalene in air or, diameter of a circular cylinder
H	height of test section, = 45.7 cm
h_m	mass transfer coefficient
L	distance from turbulence generator to cascade entrance
L_a	dimensionless length scale, $= (L_x/D)\sqrt{a_1 Re_D}$
L_x	longitudinal integral length scale
M	mesh size of turbulence generators, see Table 2
Nu	Nusselt number based on chord length
Nu_a	effective stagnation Nusselt number, $= Nu_D/\sqrt{a_1 Re_D}$
Nu_D	Nusselt number based on cylinder diameter
n	power index used in heat/mass transfer analogy
P	pitch of cascade, = 13.8 cm
Pr	Prandtl number
Re	Reynolds number based on chord length, $= UC/\nu$
Re_D	cylinder Reynolds number based on diameter and incoming velocity, $= U_{in}D/\nu$
S_p	surface distance on pressure side starting at blade leading edge
S_s	surface distance on suction side starting at blade leading edge
Sc	Schmidt number $= \nu/D$, taken to be $\sim$2.285 for naphthalene
Sh	Sherwood number based on blade chord $= h_m C/D$
Tu	turbulence intensity
Tu_a	modified turbulence intensity, $= Tu\sqrt{Re_D/a_1}$
U	average freestream velocity
U_c	average freestream velocity measured at midspan
W	width of test section, = 45.7 cm, see Fig. 1
X_c	distance upstream from the cascade entrance, see Fig. 1
X_M	distance from turbulence grids, or from the center of the second row of wall jets for high turbulence generator
X_n	longitudinal axial coordinate, see Fig. 2
x	surface distance from stagnation line, in equation for a_1
Y_n	transverse axial coordinate, see Fig. 2

Greek Symbols

β_1	inlet flow angle, = 35°
β_2	exit flow angle, = -72.49°
ν	kinematic viscosity of air

Subscripts

in	inlet condition
ex	exit condition
∞	local main flow condition along surface distance

Presented at the International Gas Turbine & Aeroengine Congress & Exhibition
Stockholm, Sweden — June 2–June 5, 1998
This paper has been accepted for publication in the Transactions of the ASME
Discussion of it will be accepted at ASME Headquarters until September 30, 1998

INTRDDUCTION

Developing more efficient and powerful gas turbines has been a goal of both designers and researchers for decades. This can be accomplished by running at higher operating temperatures, but care must be taken to account for potential heat transfer problems on surfaces within the turbine. Following the combustor, the turbulence-level entering a blade row is high and causes early boundary layer transition along the blade surfaces and enhances heat transfer there. The role of the turbulence length scale, another important parameter in a turbulent field, however, is not yet well understood. Most of the experiments related to elevated freestream turbulence have been conducted in a turbulent field generated by grids. These grids generate relatively small scales of turbulence in which the effect of scale on a blade surface has been generally ignored. Goldstein et al. (1983) found turbulence intensity of about 15-20% at the exit of can-type combustors. They found the profiles of the velocity, turbulence intensity and temperature are fairly flat at the exit of the combustor. They did not measure the length scale for those flows.

Flow across cylinders under the influence of elevated freestream turbulence, is similar to leading edge flow over a turbine blade. The correlation, given by Kestin and Wood (1971), for cylinder stagnation heat transfer in the presence of freestream turbulence does not include the influence of turbulence length scale. It works well for small turbulence length scales, but fails for larger length scales. Ames and Moffat (1990) and Ames (1997) used the combination of Reynolds number, turbulence intensity and an energy length scale to correlate their data, which seems to give a satisfactory fit. The correlation implies that a larger length scale would diminish heat transfer, but not as significantly as the turbulence intensity augments heat transfer. Dullenkopf and Mayle (1995) used von Karman's energy spectrum theory of the inertial subrange of turbulence to develop a semi-empirical correlation of Nusselt number which combines Reynnlds number, integral length scale and local acceleration factor into an "effective" turbulence intensity. The relation is linear and has the advantage that it applies not only to the stagnation region, but also to laminar boundary layers.

Grid turbulence generators are often used to increase the freestream turbulence. Baines and Peterson (1951) reported that approximately 10%, nearly isotropic turbulence, could be reached with grid turbulence generators at about 30 bar diameters downstream of the grid. Some attempts have been made to generate much higher freestream turbulence to approach the real turbine conditions. Young et al. (1992) used a jet-grid, with jets directed upwind or downwind, to generate high freestream turbulence. Thole et al. (1994) generated nearly 20% relatively large scale turbulence using opposing wall jets separated by a splitter plate in the center of their flow passage.

Combustor simulators have also been used to generate high turbulence with large-scale (Ames and Moffat (1990) and Chung and Simon (1993)). The main concern with these high turbulence generators is the uniformity of the incoming velocity, turbulence intensity and length scale. Ames and Moffat (1990) used the simulator to generate high freestream turbulence intensity and large length scale to investigate their effect on heat transfer from a cylinder and to a flat plate turbulent boundary layer. They found that large length scale reduced heat transfer near the cylinder stagnation line and to the turbulent boundary layer. Later Ames (1997) used a similar combustor simulator and a grid to generate different length scales of turbulence to investigate the effect of high turbulence on turbine vane surfaces. He found there is no significant variation of Stanton number for a turbulent boundary layer where a slightly adverse pressure gradient prevails in all the high turbulence tests in contrast to the augmentation of heat transfer in the accelerated laminar boundary layer. His data also showed that near the leading edge of his vane, the heat transfer rate with lower turbulence intensity and smaller scale is actually slightly higher than that with higher turbulence intensity and larger length scale for the two Reynolds numbers studied. Unlike many investigators, he found that the location of boundary layer transition is almost unchanged with increasing high freestream turbulence.

In the present study, a high turbulence generator, similar to a combustor simulator, along with conventional grids, are used to generate high turbulence with large length scales. The naphthalene sublimation technique is used to investigate the effect of the turbulence on transfer coefficients on simulated blade surfaces. This method has a well defined boundary condition and the results can be readily converted through the heat and mass transfer analogy (Eckert, 1976). The mass transfer technique produces very detailed local measurements and the result represents purely the fluid transport phenomena, without extraneous conduction and radiation effects that are present in heat transfer studies. A detailed description of the mass transfer technique using naphthalene sublimation including its advantages and disadvantages, is given by Goldstein and Cho (1995).

EXPERIMENTAL APPARATUS

Wind Tunnel and Test Section

The wind tunnel is the same as used for the flow visualization experiments by Wang et al. (1997). It is a multi-purpose blowing type wind tunnel, powered by a 22.4 kW blower. The air flow enters the test section through a square contraction with an area ratio of 6.25 and with exit dimensions of 45.7×45.7 cm^2.

The test section after the contraction is shown in Fig. 1. All the walls of the test section are made of 1.9 cm thick Plexiglas so that the flow in and around the cascade can be viewed to permit flow visualization experiments. The cascade contains four blades plus two bypass flexible walls. The two central blades are interchangeable to accomplish the experiments on either the pressure side or the suction side of the blades. Blade position 2 (see Fig. 1) is used for suction side tests and the position 3 for pressure side tests. The other two outside blades are fixed in position in the cascade. The two tailboards behind the two outside blades and the flexible walls can be adjusted while monitoring the static pressure to balance the flow distribution in the central passage with the neighboring passages. This produces uniform flows through the three passages. The geometry of the central passage of the cascade is illustrated in Fig. 2. The cascade dimensions and flow conditions are listed in Table 1.

Table 1: Cascade and Test Section Data.

Number of blades	4
Chord length of blade - C	18.4 cm
Axial chord of blade - C_x	13.0 cm
Pitch of cascade - P	13.8 cm
Height of cascade - H	45.7 cm
Width of wind tunnel - W	45.7 cm
Aspect ratio (Span/Chord) - H/C	2.48
Blade inlet angle - β_1	35°
Blade outlet angle - β_2	−72.49°
Inlet/Exit area ratio of the cascade	2.72
Area ratio of the contraction	6.25
Highest exit Reynolds number - Re_{ex}	7.8×10^5

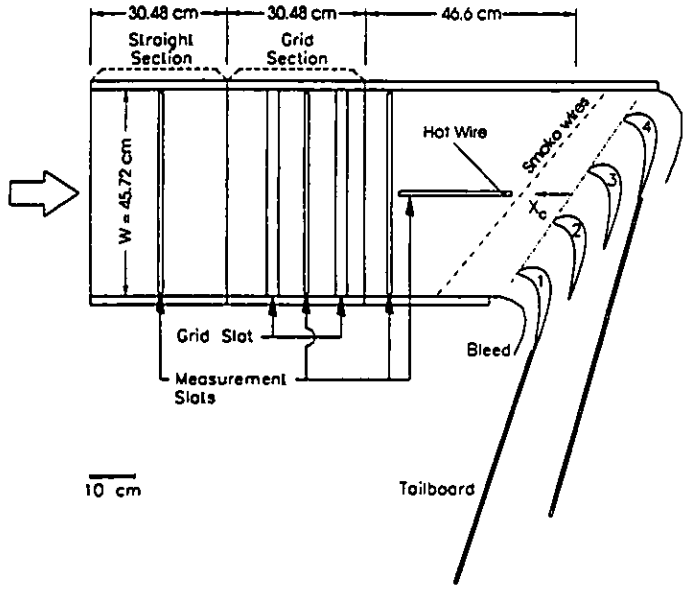

Figure 1: Schematic top view of the test section.

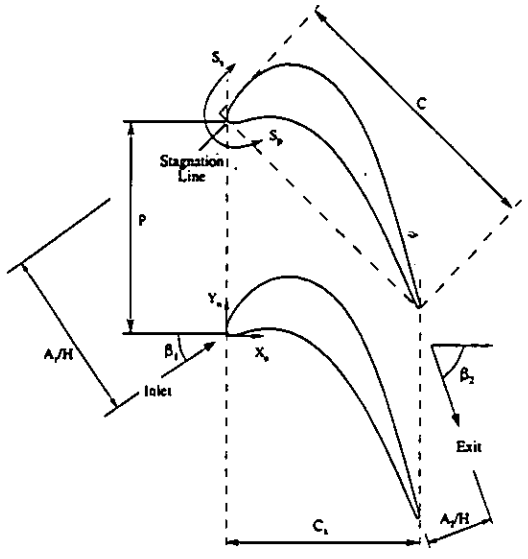

Figure 2: Central passage of the cascade and dimensions.

One of the two straight sections ahead of the cascade has two slots which can be used to insert turbulence grids to generate freestream turbulence. The straight and grid sections are interchangeable and with the grids can be used to provide different turbulence levels at the entrance of the cascade. Several slots and holes are cut into the walls ahead of and behind the cascade to insert probes to measure pressure, velocity and temperature.

Test Blades

There are two test blades: one is a pressure measurement blade used to determine the static pressure distribution on the blade surface and the other is a naphthalene blade used for mass transfer measurements. The blade profile, supplied by General Electric Co., is listed in Wang et al. (1997).

The pressure measurement blade is a hollowed-out aluminum blade. There are thirty pressure taps, of which twenty-five are used during flow balancing measurements. The static pressure distribution is measured at mid-span with the pressure measurement blade in position 2 and position 3, as shown in Fig. 1. The tailboards and bleeds are adjusted so that the measurements at the two blade locations match one another and match a potential flow calculation for the blade passage.

The second test blade, the naphthalene blade, is also made from aluminum and has two metal caps on each end which border the cast naphthalene in between. The middle part of the test blade is depressed about 2.5 mm. Melted naphthalene is cast, using a well-polished mold, into this gap to provide the same profile as the metal caps.

The pressure measurement and naphthalene blade segments are each 19.7 cm in length. The balance of the total blade length (and tunnel height) of 45.7 cm is made of two 13 cm long blade segments. When conducting a two-dimensional test, the two solid segments are positioned at the top and bottom endwalls sandwiching the test blade in between. The total length of the three blade-pieces has the same height as the wind tunnel. The three blades are held in place by two rods passing through the blades to the top and bottom walls. Two pin holes near the leading and trailing edge are drilled into the bottom endwall and the blade top and bottom caps to align the three blade pieces in position.

Turbulence Generators

Two grid turbulence generators are used to generate freestream turbulence. They can be inserted into the slots ahead of the cascade. One is an expanded metal sheet and the other is a conventional cross-bar grid made from wood. Their open area ratios are 0.56 and 0.60, respectively. The original squared bar grids are routed to a relatively round bar with two different radii. The side with larger radius faces the oncoming flow and the other side with smaller radius faces downstream. More detailed information is available in the dissertation by Wang (1997).

The third turbulence generator, shown in Fig. 3, simulates the flow from a turbine combustor. The prototype of such simulator comes from Ames and Moffat (1990) and Chung and Simon (1993). In their designs, the simulators are followed by a small contraction to get a more uniform incoming turbulent flow. To simplify the design the current high turbulence generator does not have that contraction.

Figure 3(a) is the top view of the high turbulence generator. Its main components are the front panel and two side walls, shown in Figs. 3(b-c), respectively. The front panel has four slots, two along each side in parallel. The combination of the solid block in the middle and the slots along the sides will produce a large swirling flow. Each of the two side walls has two rows of holes which inject air into the main stream to further enhance the flow circulation. The rows of small holes on the side walls were originally designed to simulate film cooling flow. However, in these tests the holes are blocked with tape and no flow comes out from the small holes. This high turbulence generator is placed ahead of the test section, Fig. 1. Two guide vanes are added at the exit of the front slots to force the flow to move along the sides. In addition, several screens are added to reduce the wall jet flows at the place where the air flow enters the side wall gaps. Relatively uniform velocity and turbulence distributions are obtained in both the vertical and horizontal directions with this system ((Wang, 1997)).

Data Acquisition Systems

The turbulent field is measured using a TSI Model 1210 single-sensor, hot-wire probe and TSI IFA 100 system. The flow and blade temperatures are measured using Copper-Constantan (Type T) thermocouples. The integral length scale of turbulence is computed from Tay-

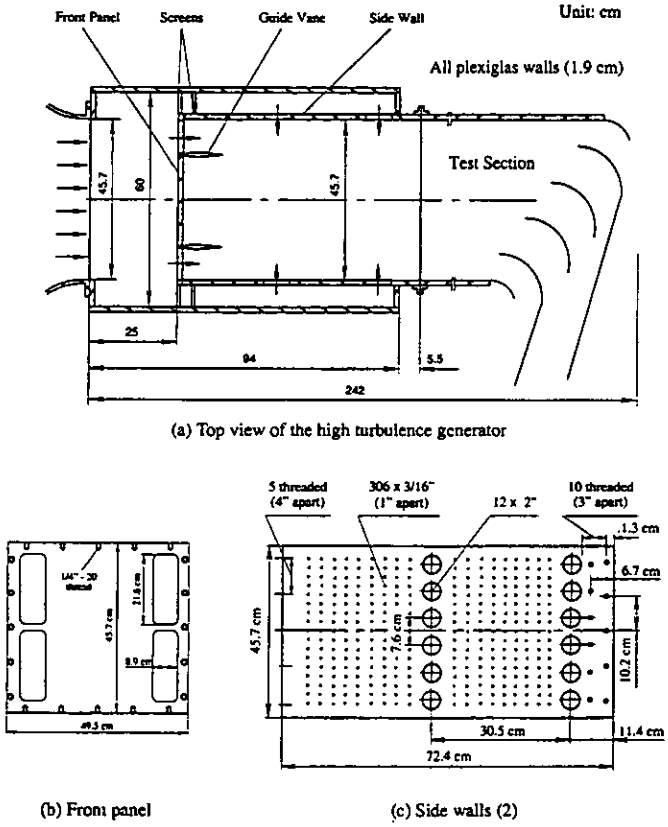

Figure 3: Large scale high turbulence generator.

lor's hypothesis by averaging 30 sets of power spectrum sampling data, acquired at a 20 kHz sampling rate with a cutoff frequency of 10 kHz, and using an autocorrelation function.

The data acquisition system used in the naphthalene mass transfer experiments is generally the same as described in the paper by Goldstein et al. (1995). The measurement tables have been refurbished to meet the need of scores of tests and the computer has been upgraded. Nearly 3,000 data points can be taken in an hour. The uncertainty of the results, at 95% confidence using the methods described by Kline and McClintock (1953), is about 7% in Sherwood number measurement, of which 5~6% comes from the uncertainty in property correlations. As a result, the relative error would be much smaller.

A typical naphthalene sublimation wind tunnel test takes about 40 to 60 minutes during which about 0.08 mm naphthalene in average depth is sublimed. This amount naphthalene sublimation generally does not affect the flow field around the blade.

RESULTS OF FLOW FIELD MEASUREMENT

Static Pressure Distribution In the Passage

The static pressure is measured along the suction and pressure surfaces at the mid-span inside the central passage of the cascade using a special blade section with twenty-five pressure taps. The measured distribution is shown in Fig. 4. The static pressure distributions along the two adjacent passages are also measured to compare with the central passage measurement. It is seen from the figure that the neighboring passages have almost the same pressure distributions as the central passage. The solid lines in the figure are the results calculated from potential flow theory and match quite well with the measurements. The three

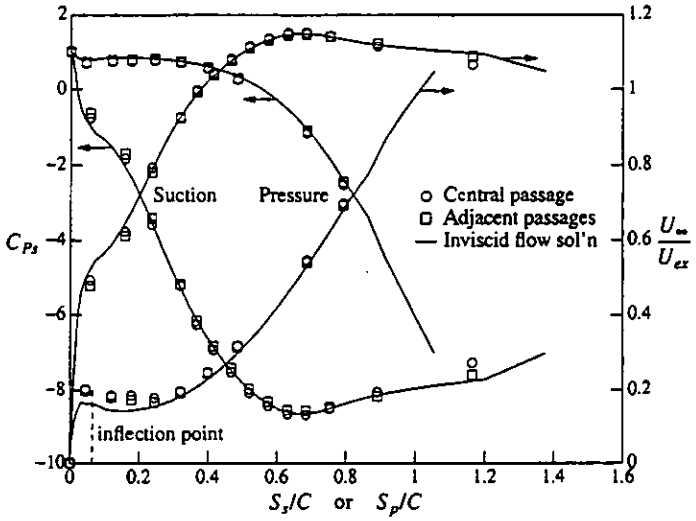

Figure 4: Static pressure coefficient and velocity profiles along blade surfaces at $Re_{ex}=5.2\times10^5$, $U_{ex}/U_{in}=2.7$.

passages between the two tailboards have almost the same volumetric flows. The flow inside the central passage is expected to represent the flow in a continuous blade cascade.

Based on the pressure distribution along the blade surfaces, a corresponding velocity distribution can be calculated using the Bemoulli equation. Figure 4 also shows the local freestream velocity distribution along the surface distance, normalized by the exit velocity. The velocity profile computed from the potential flow theory can be used to define a local similarity variable, m, which is used to solve the local laminar wedge-flow similarity equations of momentum, heat and mass transfer. The approximate analytical method is described in Goldstein et al. (1995).

Incoming Flow Profiles

The spanwise distributions of the incoming velocity, turbulence intensity and integral length scale for each of the three turbulence generators as well as for the low turbulence case, are shown in Fig. 5. These are measured at $X_c/C=0.8$. All the distributions are quite uniform along the span of the cascade. The turbulence decay and the length scale growth are plotted in Fig. 6. The decay/growth of turbulence/length-scale are measured by moving the grids upstream to obtain the turbulent field for the corresponding cascade position. For the high turbulence generator, the flow condition at the cascade entrance is extrapolated from its decay/growth curve. The data are summarized in Table 2. The values represent the flow conditions at a distance equal to the center of the cascade and would be slightly different at Blade positions 2 and 3. No measurable difference in mass transfer was found at the stagnation points for the two blade positions, however.

Producing uniform velocity and turbulence profiles for the high tur-

Table 2: Cascade-entrance Free-stream Turbulence Parameters, $X_c = 0$.

Generator	Tu(%)	L_x(cm)	M(cm)	L(cm)
No grid	0.2	-	-	-
Expanded Metal Sheet	3.0	0.9	1.27	51.0
Bar Grid of 2 cm	8.5	2.6	9.00	102.2
High Tu Generator	18.0	8.0	7.62	119.1

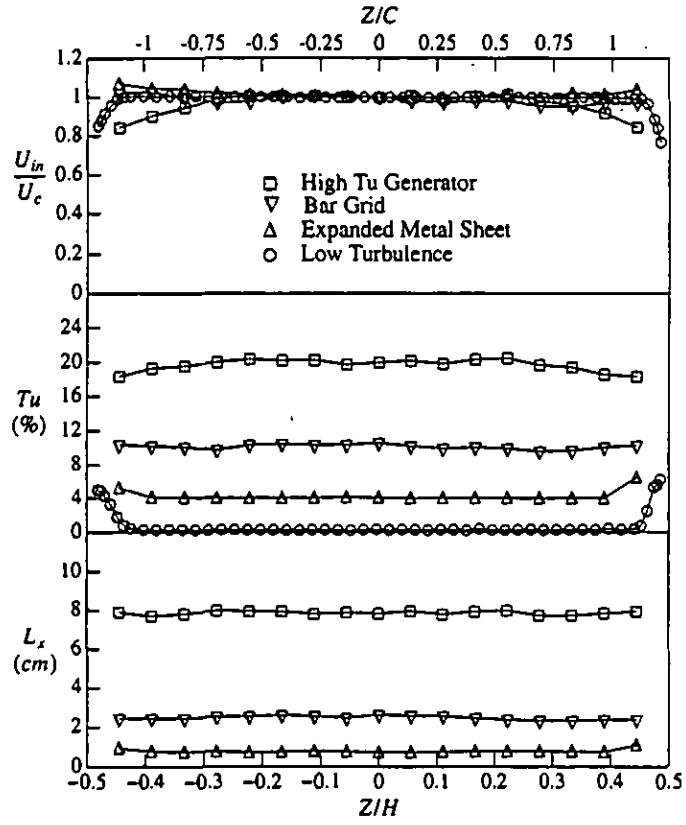

Figure 5: Spanwise incoming velocity profiles measured at $X_c/C = 0.8$ with and without turbulence generators ($Re_{ex} = 5.2 \times 10^5$).

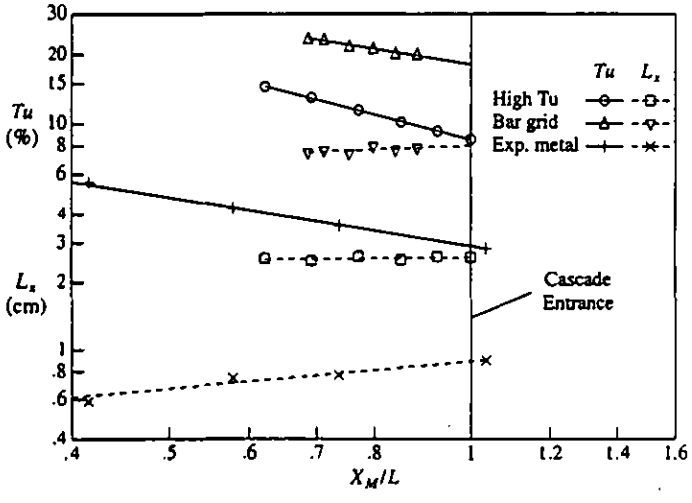

Figure 6: Decay/Growth of turbulence/scales of different turbulence generators.

bulence generator is difficult. Before installing the guide vanes at the exit of the front panel slots (Fig. 3a), the measurement in the lateral direction showed a parabolic velocity profile, with the highest velocity in the middle. After installing the guide vanes and adjusting the wall jets, a relatively uniform velocity profile in the lateral direction is obtained at $X_c/C = 2.3$ ($X_M/M = 10.2$) with 4.5% variation in velocity and less than 10% variation in turbulence and length scale. The lateral distributions of velocity and turbulence parameters are very similar to the vertical

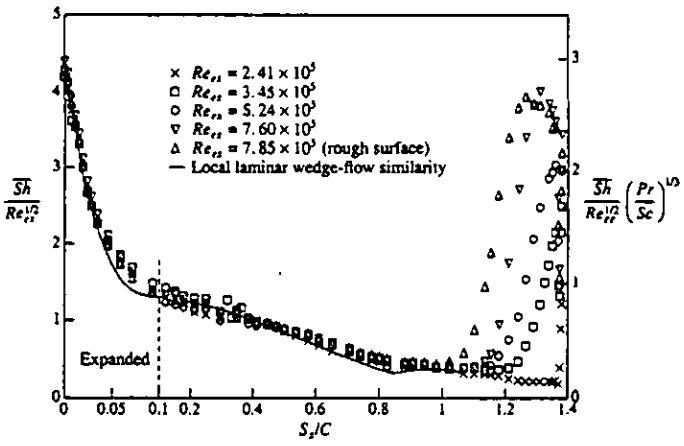

Figure 7: Comparison of $\overline{Sh}/Re_{ex}^{1/2}$ along the suction surface at different Re_{ex}'s (low turbulence).

distributions of Fig. 5. For detailed upstream information about power spectra, autocorrelation and flow uniformity of the flow parameters on these turbulence generators, readers should refer to Wang (1997).

MASS TRANSFER RESULTS AND DISCUSSION

Reynolds Effect at Low Free Stream Turbulence

Tests are performed at four Reynolds numbers over the range $2.4 \times 10^5 < Re_{ex} < 7.8 \times 10^5$. The mass transfer results along the suction surface are shown in Fig. 7 using the dimensionless laminar flow parameter $Sh/Re^{1/2}$. Also shown in the figure are the local laminar wedge-flow similarity solutions for comparison. The mass transfer results on the pressure side in the absence of freestream turbulence vary due to the development of Taylor-Görtler vortices. This issue is discussed in a forthcoming paper.

It is seen (Fig. 7) that in the region from $S_s/C < 1.05$, all the data fall on one curve and match well with the local laminar wedge-flow similarity solution. It appears that the flow regime is laminar over most of the suction surface for the Reynolds number range studied. Higher transfer rates are found both near the leading edge ($S_s/C \approx 0$) and near the trailing edge ($S_s/C > 1$) where boundary layer transition occurs for higher Reynolds numbers. When the Reynolds number is small ($Re_{ex} = 2.4 \times 10^5$) it appears that boundary layer transition does not occur until very near the trailing edge. The rapid rise in Sherwood number at the trailing edge indicates the vortex shedding behind the blade. With increasing Reynolds numbers the start of boundary layer transition gradually moves upstream, but the transition is not complete by the trailing edge for $Re_{ex} < 7.6 \times 10^5$.

Also included in Fig. 7 is a second test at $Re_{ex} = 7.85 \times 10^5$. A rather rough surface finish due to poor casting near the trailing edge ($S_s/C > 1$) in the test is the main difference from the other run at this Reynolds number. These two tests are very repeatable except for the location of transition. As indicated by the mass transfer Sherwood number, the boundary layer flow with the rough surface has an earlier boundary layer transition than that with a relatively smooth surface.

Effect of Turbulence

Two Reynolds numbers (3.6×10^5 and 5.2×10^5) tests are performed with high incoming freestream turbulence in the central passage of the cascade. Figures 8–9, show the distributions of mass transfer Sherwood number along the suction and the pressure surfaces when the

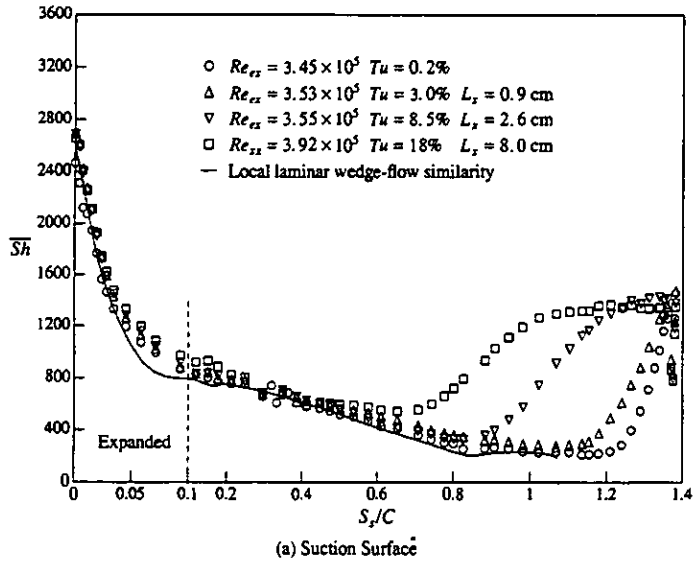

(a) Suction Surface

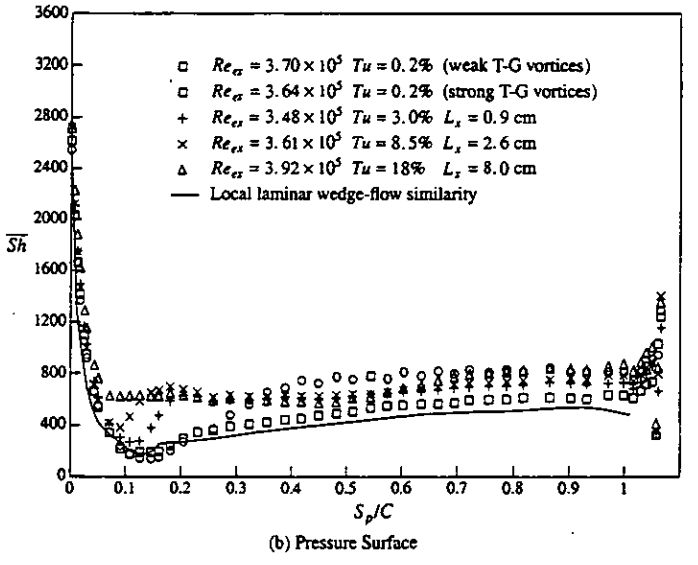

(b) Pressure Surface

Figure 8: Sherwood number distribution for elevated turbulence levels at $Re_{ex} = 3.6 \times 10^5$.

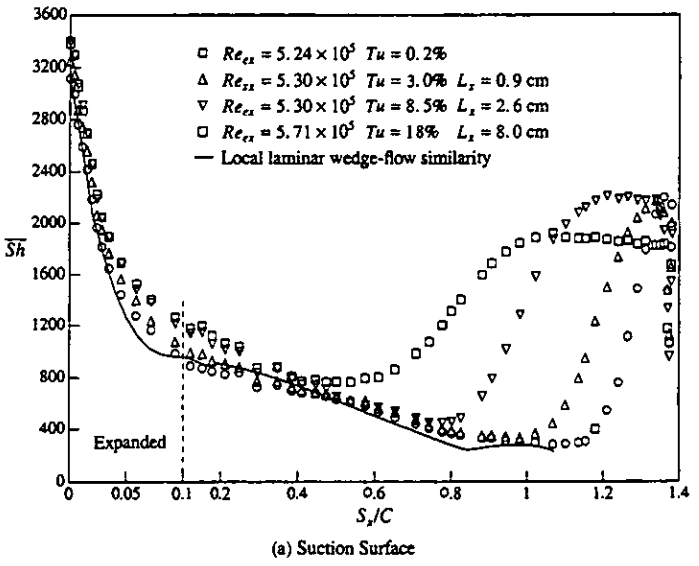

(a) Suction Surface

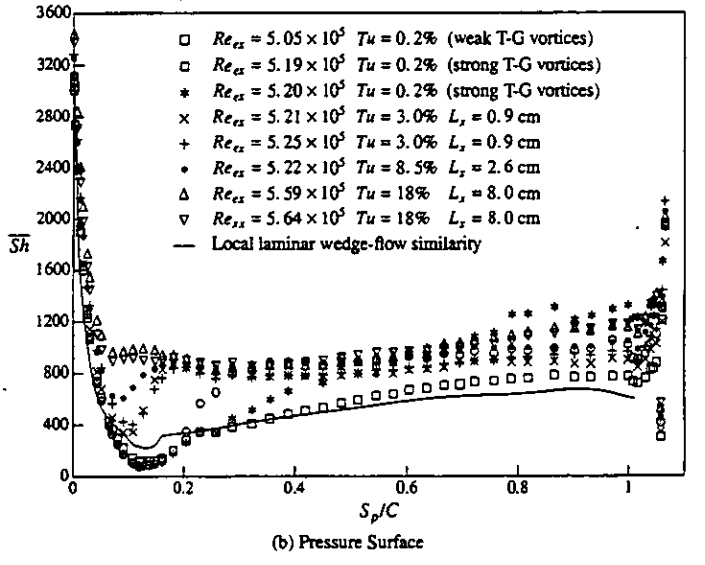

(b) Pressure Surface

Figure 9: Sherwood number distribution for elevated turbulence levels at $Re_{ex} = 5.2 \times 10^5$.

test blade is exposed to different incoming freestream turbulence.

On the suction surface at $Re_{ex} = 3.6 \times 10^5$, there is almost no effect of high free stream turbulence on the mass transfer in the laminar boundary layer region. The Sherwood number matches well with the local laminar similarity solution even though the freestream turbulence intensity is raised as high as 18%. When the Reynolds number reaches 5.2×10^5, a slightly higher mass transfer rate is observed around $S_s/C = 0.18$ with increasing turbulence level, but the boundary layer is still laminar.

An interesting impact of elevated turbulence is the bypass-type, early boundary-layer transition. The start of transition shifts upstream with increasing turbulence level. When the turbulence level reaches $\approx 18\%$, the region with transition or a turbulent boundary layer covers about half of the blade suction-surface. In addition, higher Reynolds numbers would move the start of transition even farther upstream and more blade surface would be exposed to a turbulent boundary layer. This transition and the subsequent turbulent boundary layer significantly increase the mass transfer rate, compared to the results in the same area with a laminar boundary layer.

It is hard to determine from these limited tests how the length scale affects the boundary layer transition. It is seen from Fig. 8–9 that when the freestream turbulence is less than 8.5%, the boundary layer transition starts in the decelerated region ($S_s/C > 0.8$, c.f. Fig. 4) while for the case of the high-turbulence generator ($Tu = 18\%$), it starts near the narrowest width (highest acceleration at $S_s/C \approx 0.65$) of the channel. Interestingly, the integral length scale of the latter ($L_x = 8$ cm) is roughly equivalent to the size of the blade passage. Actually the narrowest width of the channel (~ 6 cm) is even smaller than the length scale. Also a longer length of boundary layer transition is found with increasing turbulence level, as indicated by the mass transfer results. More studies are needed to explore the effect of length scale on the boundary layer transition in this complicated accelerated/decelerated flow.

For $Re_{ex} = 3.6 \times 10^5$ (Fig. 8a), the mass transfer rates in the turbulent boundary layer region after transition are almost independent of freestream flow conditions. For $Re_{ex} = 5.2 \times 10^5$ with 18% freestream turbulence (Fig. 9a), however, a lower mass transfer rate close to the trailing edge has been found than occurs for 3% and 8.5% turbulence at large S_s/C. The reduction of mass transfer is about 15%. This suggests that, except for an early boundary layer transition, elevated freestream turbulence may not necessarily produce higher mass transfer in the turbulent boundary layer. On the other hand, the large length scale may play a role in reducing the mass transfer rate in the turbulent boundary layer.

On the pressure surface, the mass transfer rate reaches a minimum near $S_p/C = 0.12$ after the blade inflection point ($S_p/C = 0.065$) with low freestream turbulence. With increasing turbulence levels, the minimum gradually moves upstream and almost vanishes when the turbulence level reaches 18% with an integral length scale of about 8 cm. The incoming turbulence significantly enhances the mass transfer rate locally around $S_p/C = 0.1$, compared to the extremely low mass transfer rate with low freestream turbulence.

For low freestream turbulence intensity tests, Taylor-Görtler vortices develop on the pressure surface and can significantly enhance the mass transfer rate. In the presence of elevated freestream turbulence, no Taylor-Görtler vortices have been observed on the pressure surface in any of the mass transfer tests. It is interesting to see from the figures that the mass transfer rate is not as strongly enhanced by the freestream turbulence as it is by Taylor-Görtler vortices in the low turbulence case. This issue will be discussed in a forthcoming paper.

It is believed that the pressure-side boundary layer remains laminar due to the strong acceleration in the cascade. However, the mass transfer rate in the presence of high freestream turbulence over the entire pressure surface is higher than predicted using the local similarity analysis. It is interesting to see that the mass transfer rates in the tests do not vary significantly with turbulence level ($Tu = 3 \sim 18\%$) except in the area immediately after the inflection point.

Comparison with Heat Transfer Results

Figure 10 shows a comparison with the heat transfer results of Mehendale et al. (1994). The geometry data reported in their paper and the present blade profile are very similar, and both profiles are acquired from General Electric Co. The main difference between the two cascades is the aspect ratio. They have a relatively short cascade with the aspect ratio (Height/Chord) about 1.1 while the present aspect ratio is about 2.5. A slightly different Pitch/Chord ratio accounts for another difference. Hence the velocity ratio is about 2.4 in their cases and is about 2.7 in the present work. A constant heat flux method was used in their experiments and their data are averaged over the whole span. Clearly their Nusselt numbers include the influence of the secondary flows from both endwalls.

In the conversion of Sherwood number to Nusselt number, the power index of $n = 1/3$ and $n = 0.4$ are used in Eq. 1 for the laminar and turbulent boundary layers respectively,

$$\frac{Nu}{Sh} = \left(\frac{Pr}{Sc}\right)^n \qquad (1)$$

A linear interpolation between 1/3 and 0.4 is used in estimating the Nusselt number in the transition zone. The present mass transfer experiment with a constant surface concentration actually represents a constant temperature case in heat transfer which accounts for another difference from a constant heat flux experiment.

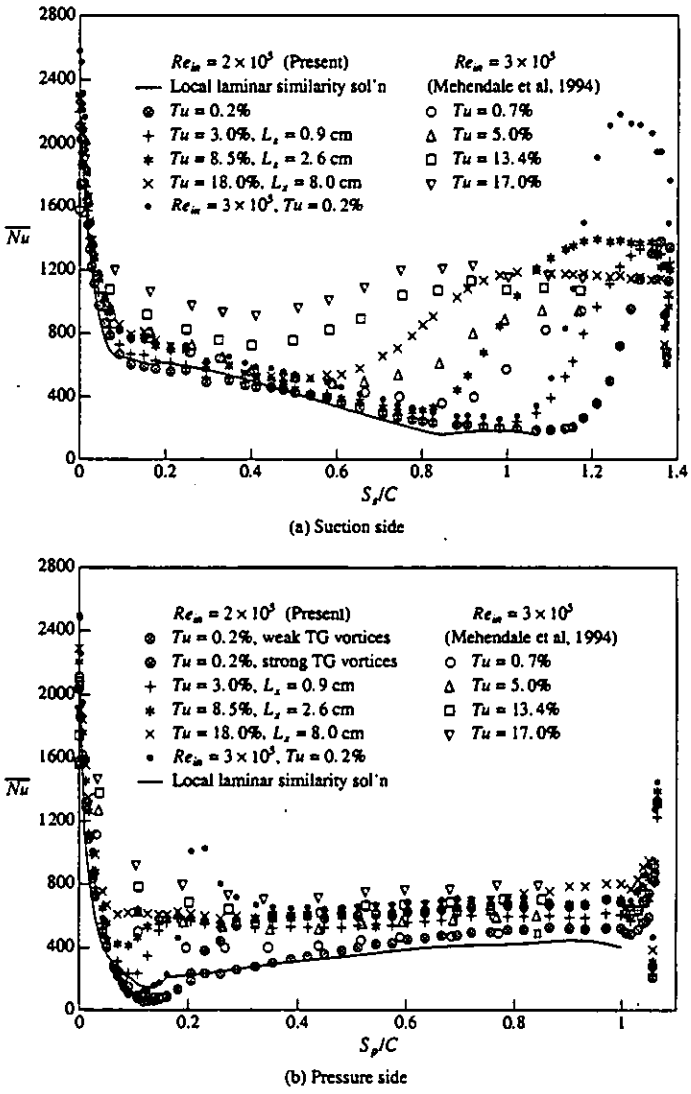

Figure 10: Present investigation compared with heat transfer results of Mehendale et al. (1994).

Since they used inlet velocity to calculate Reynolds number, a corresponding change of the current exit Reynolds number is made to match their definition. The inlet Reynolds number of the current primary turbulence tests is a little lower than theirs and only one test condition with no freestream turbulence matches their flow condition. It is seen from the figure that the general trend for these tests are basically the same. But there are some differences which need to be addressed.

The present tests have much higher Nusselt number near the leading edge than the data presented by Mehendale et al. (1994). This is probably due to conduction inside their small nose. The mass transfer has no error equivalent to conduction. The peak value is probably smoothed out by the conduction. In addition, an endwall horseshoe vortex flow around the stagnation region would affect the heat transfer from the blade surface.

On the suction side, the main feature is the early boundary layer

transition caused by freestream turbulence. In addition, much earlier transition found in Mehendale et al. (1994) could be attributed to the cascade secondary flows. It is interesting to note that for $Re_{in}=3\times10^5$ with no free stream turbulence the boundary layer transition in the current case is later compared to theirs, but the transfer rate is much higher in the present tests in the turbulent boundary layer farther downstream. This phenomenon implies that the secondary flows in their cascade may considerably thicken the turbulent boundary layer and hence reduce the heat transfer downstream.

On the pressure side in the case of $Re_{in}=3\times10^5$ with low freestream turbulence, the present results clearly show the processes of transition and relaminarization at the location around $S_p/C=0.2$. There is no valley or peak found in their Nusselt number distribution, probably due to the effect of conduction and secondary flows. In the presence of high free stream turbulence ($Re_{in}=2\times10^5$), very similar distributions of Nusselt number are obtained from both cascades.

Leading Edge Mass Transfer

The test blade has a very small leading edge nose. The flow around the stagnation line of a turbine blade is related to the flow around a circular cylinder in crossflow, but they are not exactly the same. A cylinder in crossflow usually has a laminar or turbulent boundary layer separation before the wake region, which a turbine blade near the stagnation line does not have. The boundary layer around the stagnation line of a blade is actually a little thicker than the boundary layer of a cylinder even though they may have the same nose size. In other words the stagnation flow around a cylinder with an effective nose size, larger than the real size of blade nose, could be adopted to simulate the flow around the stagnation line of blade. If the blade nose is large the effective size may be close to the real size. Since the current test blade has a very small nose, about 3 mm in diameter, caution must be taken when comparing to measurements on circular cylinders. Choosing a cylinder with calculated flow acceleration data and the local similarity solution, indicates an effective cylinder of 9 mm diameter.

Kestin and Wood (1971) suggested a correlation of Nusselt number for stagnation flow around a cylinder in the presence of high freestream turbulence.

$$\frac{Nu}{Re_D^{1/2}}=0.945+3.48\left(\frac{TuRe_D^{1/2}}{100}\right)+3.99\left(\frac{TuRe_D^{1/2}}{100}\right)^2 \qquad (2)$$

The correlation and the effective nose Nusselt number with elevated turbulence are shown in Fig. 11. It is seen from the figure that for relatively low freestream turbulence the data match reasonably well with the correlation. For higher freestream turbulence with large length scale the data is well off the correlation line; Kestin's correlation does not consider the effect of length scale.

The correlation suggested by Dullenkopf and Mayle (1995), includes both effect of turbulence intensity and integral length scale.

$$Nu_a Pr^{-0.37}=0.571+0.01Tu_\lambda \qquad (3)$$

where,

$$Tu_\lambda=\frac{Tu_a L_a^{1/2}}{(1+0.004L_a^2)^{5/t2}}$$

They used a more general acceleration parameter as a characteristic length and combined turbulence and length scale into an effective turbulence intensity. The comparison of the current experimental nose Nusselt numbers with the correlation is shown in Fig. 12. The data fit well with the correlation for moderately high turbulence and length scales. The data with large length scales are a bit off probably because the correlation may not fit well with extremely large scales as indicated by the authors.

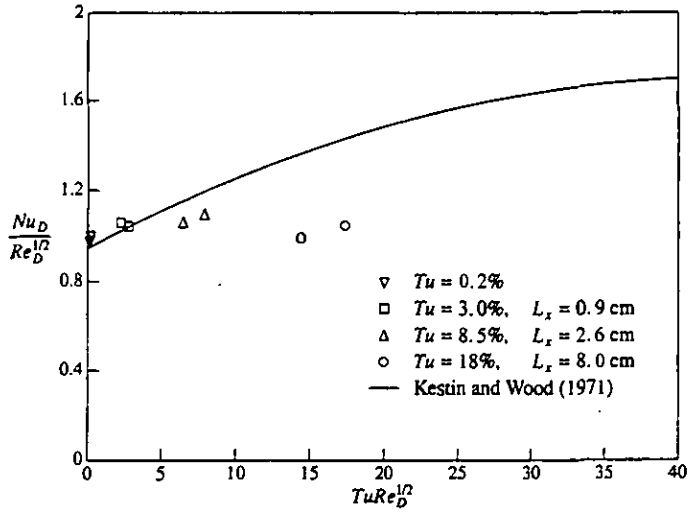

Figure 11: Nusselt number at the leading edge of turbine blade, compared to the cylinder correlation by Kestin and Wood (1971).

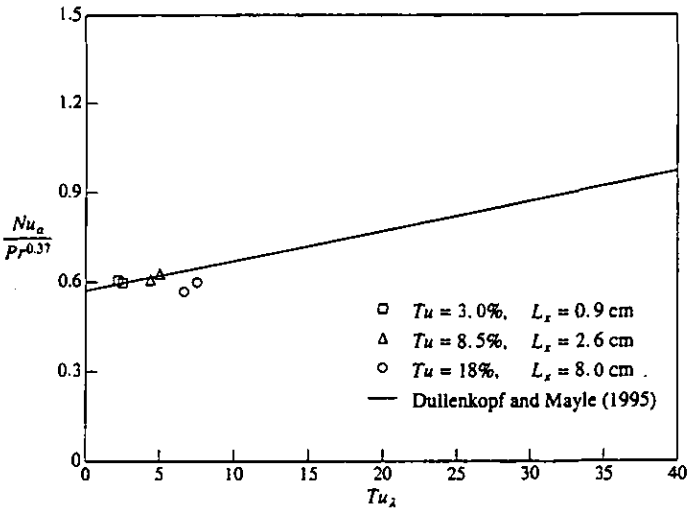

Figure 12: Nusselt number at the leading edge of turbine blade, compared to the cylinder correlation by Dullenkopf and Mayle (1995).

It must be mentioned that the dimensionless acceleration parameter a_1 in the equation may vary from 2.4 to 4, with the latter number a potential flow parameter. The above stagnation data is obtained using $a_1=3.8$. As pointed out by the authors the parameter a_1 is a function of many factors including the length scale. It is worth mentioning that the current data would fit well with the correlation if a_1 is reduced for high turbulence and large length scale or if a_1 increases for relatively low turbulence and small length scale.

CONCLUSIONS

(1) High freestream turbulence with large length scale can be produced using a high turbulence generator (combustor simulator). A quite

uniform incoming velocity and turbulent field has been obtained for the subsequent tests involving high freestream turbulence.

(2) Due to the strong acceleration of the passage flow, most of the suction and pressure surfaces are dominated by a laminar boundary layer for low freestream turbulence. When Reynolds number is extremely low, $Re_{ex} < 2.4 \times 10^5$, essentially no transition has been observed on the suction surface.

(3) The freestream turbulence, by contrast, has little effect on the laminar boundary layer on the suction surface. The main contribution of freestream turbulence is to cause an early boundary layer transition to turbulence, leading to a several fold increase in mass transfer compared to the corresponding laminar boundary layer.

(4) In the turbulent boundary layer on the suction surface, high turbulence intensity may not necessarily produce higher mass transfer rate. The length scale may have a considerable impact on mass transfer in reducing the transport rate. Attention to length scale should be paid at least equally with turbulence intensity to understand better the effect of freestream turbulence.

(5) Caution should be taken when comparing the blade leading edge data to cylinder data. The flows are not exactly the same for the two geometries, especially for a blade with a small nose at the leading edge. The correlation presented by Dullenkopf and Mayle (1995) includes the effect of both turbulence level and length scale and correlates the present data relatively well. More experiments are needed to document the information, particularly on large length scale, together with turbulence intensity.

ACKNOWLEDGMENTS

We wish to thank the Advanced Gas Turbine Systems Research (AGTSR) Program funded by the United States Department of Energy and the Industrial Review Board Membership for their support and contract monitor Dr. Daniel Fant for his continued interest in our research. This paper was prepared with the support of the U. S. Department of Energy, Morgantown Energy Technology Center, Cooperative Agreement No. DE-FC21-92MC29061.

REFERENCES

Ames, F. E., 1997. "The Influence of Large-Scale High-Intensity Turbulence on Vane Heat Transfer." *Journal of Turbomachinery*, vol. 119, pp. 23–30.

Ames, F. E. and Moffat, R. J., 1990. "Heat Transfer With High Intensity, Large Scale Turbulence: The Flat Plate Turbulent Boundary Layer and the Cylindrical Stagnation Point." In *NASA Report No.HMT-44*. Department of Mechanical Engineering, Stanford University, Stanford, CA.

Baines, W. D. and Peterson, E. G., 1951. "An Investigation of Flow Through Screens." *Transaction of the ASME*, vol. 73, pp. 467–480.

Chung, J. T. and Simon, T. W., 1993. "Effectiveness of the Gas Turbine Endwall Fences in Secondary Flow Control at Elevated Freestream Turbulence Levels." *ASME Paper 93-GT-51*.

Dullenkopf, K. and Mayle, R. E., 1995. "An Account of Free-Stream-Turbulence Length Scale on Laminar Heat Transfer." *Journal of Turbomachinery*, vol. 117, pp. 401–406.

Eckert, E. R. G., 1976. "Analogies to Heat Transfer Processes." In E. R. G. Eckert and R. J. Goldstein, editors, *Measurement in Heat Transfer*, pp. 397–423. Hemisphere, New York.

Goldstein, R. J. and Cho, H. H., 1995. "A Review of Mass Transfer Measurements Using Naphthalene Sublimation." *Experimental Thermal and Fluid Science*, vol. 10, pp. 416–434.

Goldstein, R. J., Lau, K. Y., and Leung, C. C., 1983. "Velocity and Turbulence Measurements in Combustion Systems." *Experments in Fluids*, vol. 1, pp. 93–99.

Goldstein, R. J., Wang, H. P., and Jabbari, M. Y., 1995. "The Influence of Secondary Flows Near the Endwall and Boundary Layer Disturbance on Convective Transport From a Turbine Blade." *Journal of Turbomachinery*, vol. 117, pp. 657–665.

Kestin, J. and Wood, R. T., 1971. "The Influence of Turbulence on Mass Transfer From Cylinders." *Journal of Heat Transfer*, vol. 93, no. 4, pp. 321–327.

Kline, S. J. and McClintock, F. A., 1953. "Describing Uncertainties in Single Sample Experiments." *Mechanical Engineering*, vol. 75, pp. 3–8.

Mehendale, A. B., Ekkad, S. V., and Han, J. C., 1994. "Mainstream Turbulence Effect on Film Effectiveness and Heat Transfer Coefficient of a Gas Turbine Blade With Air and CO_2 Film Injection." *International Journal of Heat and Mass Transfer*, vol. 37, no. 17, pp. 2707–2714.

Thole, K. A., Bogard, D. G., and Whan-Tong, J. L., 1994. "Generating High Freesteam Turbulence Levels." *Experiments in Fluids*, vol. 17, pp. 375–380.

Wang, H. P., 1997. "Local Mass Transfer Measurement from a Turbine Blade: Influence of High Turbulence with Large Length Scale on Heat/Mass Transfer." Ph.D. dissertation, University of Minnesota, Minneapolis, Minnesota.

Wang, H. P., Olson, S. J., Goldstein, R. J., and Eckert, E. R. G., 1997. "Flow Visualization in Linear Turbine Cascade of High Performance Turbine Blades." *Journal of Turbomachinery*, vol. 119, pp. 1–8.

Young, C. D., Han, J. C., Huang, Y., and Rivir, R. B., 1992. "Influence of Jet-Grid Turbulence on Flat Plate Turbulent Boundary Layer Flow and Heat Transfer." *Journal of Heat Transfer*, vol. 114, pp. 65–72.